

# Supplementary Material: Cadmium and Lead Adsorption/Desorption on Non-Amended and by-Product-Amended Soil Samples and Pyritic Material

Avelino Núñez-Delgado <sup>1,\*</sup>, Aurora Romar-Gasalla <sup>1</sup>, Vanesa Santás-Miguel <sup>2</sup>, María J. Fernández-Sanjurjo <sup>1</sup>, Esperanza Álvarez-Rodríguez <sup>1</sup>, Juan Carlos Nóvoa-Muñoz <sup>2</sup> and Manuel Arias-Estévez <sup>2</sup>

## Characterization of the Materials

The forest soil samples were from an A horizon in a soil developed over granitic rocks near the Alcoa aluminum factory (San Cibrao, Lugo province, Spain). The vineyard soil was developed over schists, and it was sampled in Sober (Lugo province, Spain). The pyritic material was from a copper mine tailing (Touro, A Coruña province, Spain). The finely ground (<1 mm) mussel shells were from the Abonomar S.L. factory (A Illa de Arousa, Pontevedra province, Spain). The pine bark was a commercial product from Geolia (Madrid, Spain), where the <0.63 mm particle size fraction was used after grounding and sieving. The oak ash was from a combustion boiler in Lugo (Spain). The hemp waste, with particle size between 0.63–5 mm, was from an enterprise working on hemp-derived products, situated in Guitiriz (Lugo province, Spain).

The forest soil, the vineyard soil, and the pyritic material were sampled at 0–20 cm depth in a zigzag manner (10 subsamples taken to perform each final composite sample). All these samples were air dried and sieved through 2 mm in the laboratory, and chemical determinations were carried out on the <2 mm fraction, with all determinations being performed in triplicate.

C and N were determined on 5 g samples by means of an elemental Tru Spec CHNS auto-analyzer (LECO Corporation, St. Joseph, MI, USA) [4] pH in water was measured on 10 g of solid sample (solid: liquid relation 1 : 2.5) using a pH-meter (model 2001, Crison, L'Hospitalet de Llobregat, Barcelona, Spain) [11], also used to measure the point of zero charge ( $\text{pH}_{\text{pzc}}$ ) [12]. Exchangeable Ca, Mg, Al, Na and K were quantified by atomic absorption and emission spectroscopy (AAnalyst 200, Perkin Elmer, Boston, MA, USA) after extraction from 5 g samples with a 1 M  $\text{NH}_4\text{Cl}$  solution [20]; the effective cationic exchange capacity (eCEC) was calculated as the sum of these cations [9]. Total P was quantified on 1 g samples using UV-visible spectroscopy (UV-1201, Shimadzu, Kioto, Japan) after nitric acid (65%) microwave assisted digestion [21]. To determine total concentrations of Na, K, Ca, Mg, Al, Fe, Mn, As, Cd, Cr, Cu, Ni and Zn, a nitric acid (65%) microwave assisted digestion was carried out on 1 g samples, then quantifying by means of ICP-mass spectrometry (820-NS, Varian, Palo Alto, CA, USA) [14]. Total concentrations of non-crystalline Al and Fe ( $\text{Al}_0$ ,  $\text{Fe}_0$ ) were measured using ammonium oxalate solutions (acidified to pH 3 with oxalic acid) on 1 g samples [2]. All trials were performed by triplicate. Table S1 shows the results corresponding to the chemical characterization of the materials assayed. In addition, the particle-size distribution of forest and vineyard soil samples was determined by using the Robinson pipette procedure, giving: forest soil 65% sand, 20% silt and 15% clay; vineyard soil 73% sand, 12% silt and 15% clay.

**Table S1.** General characteristics of the sorbent materials (average values for three replicates, with coefficients of variation always <5%)

	<b>Forest soil</b>	<b>Vineyard soil</b>	<b>Pyritic material</b>	<b>Fine shell</b>	<b>Pine bark</b>	<b>Oak ash</b>	<b>Hemp waste</b>
C (%)	4.22	2.94	0.26	11.43	46.95	11.65	36.53
N (%)	0.33	0.23	0.04	0.21	0.32	0.21	2.81
pH <sub>water</sub>	5.65	4.48	2.97	9.39	3.99	11.31	8.70
pH <sub>pzc</sub>	5.53	4.14	3.46	9.94	4.00	12.52	9.00
C <sub>a</sub> e (cmol <sup>(+)</sup> kg <sup>-1</sup> )	4.37	1.78	0.36	24.75	5.38	95.03	31.15
Mg <sub>e</sub> (cmol <sup>(+)</sup> kg <sup>-1</sup> )	0.66	0.24	0.29	0.72	2.70	3.26	3.67
Na <sub>e</sub> (cmol <sup>(+)</sup> kg <sup>-1</sup> )	0.33	0.14	0.14	4.37	0.46	12.17	4.19
K <sub>e</sub> (cmol <sup>(+)</sup> kg <sup>-1</sup> )	0.60	0.83	0.24	0.38	4.60	250.7	21.82
A <sub>le</sub> (cmol <sup>(+)</sup> kg <sup>-1</sup> )	1.92	2.28	2.86	0.03	1.78	0.07	<0.001
eCEC (cmol <sup>(+)</sup> kg <sup>-1</sup> )	7.88	5.27	3.89	30.25	14.92	361.2	60.83
P <sub>T</sub> (mg kg <sup>-1</sup> )	423.9	679.3	606.3	101.5	<0.01	663.7	1935
Ca <sub>T</sub> (mg kg <sup>-1</sup> )	708.5	607.1	603.0	280168	2319	136044	13258
Mg <sub>T</sub> (mg kg <sup>-1</sup> )	830.5	5003	8384	980.6	473.6	26171	6987
Na <sub>T</sub> (mg kg <sup>-1</sup> )	515.1	297.6	412.0	5173	68.92	2950	663.0
K <sub>T</sub> (mg kg <sup>-1</sup> )	1544	5441	3186	202.1	737.8	99515	10438
As <sub>T</sub> (mg kg <sup>-1</sup> )	4.18	3.41	7.0	1.12	<0.001	8.36	0.76
Cd <sub>T</sub> (mg kg <sup>-1</sup> )	0.43	0.14	0.08	0.07	0.13	19.93	0.08
Cr <sub>T</sub> (mg kg <sup>-1</sup> )	18.35	41.44	99.0	4.51	1.88	36.28	8.66
Cu <sub>T</sub> (mg kg <sup>-1</sup> )	15.72	521.1	773.0	6.72	<0.001	146.33	18.06
Ni <sub>T</sub> (mg kg <sup>-1</sup> )	10.69	21.73	5.0	8.16	1.86	69.25	8.03
Zn <sub>T</sub> (mg kg <sup>-1</sup> )	36.74	49.57	58.0	7.66	6.98	853.0	73.86
Mn <sub>T</sub> (mg kg <sup>-1</sup> )	92.99	305.4	296	33.75	30.19	10554	577.1
Al <sub>T</sub> (mg kg <sup>-1</sup> )	22676	25664	9624	433.2	561.1	14966	2307
Fe <sub>T</sub> (mg kg <sup>-1</sup> )	9486	21284	135157	1855	169.8	12081	2061
Al <sub>o</sub> (mg kg <sup>-1</sup> )	4275	2003	563.0	178.3	315.0	8323	273.0
Fe <sub>o</sub> (mg kg <sup>-1</sup> )	2333	1239	41860	171.0	74.02	4233	322.2

X<sub>e</sub>: exchangeable concentration of the element; X<sub>T</sub>: total concentration of the element; Al<sub>o</sub>, Fe<sub>o</sub>: extracted with ammonium oxalate

### Infrared spectroscopy

In addition to the parameters commented above, some additional characteristics (including the main functional groups present in each material) were determined by infrared spectroscopy on a FTIR-Bomen MB102 equipment (ABB, Zürich, Switzerland). The spectra were obtained by transmittance using KBr pellets, performing determinations in the region between 400 and 4000 cm<sup>-1</sup>, with a resolution of 4 cm<sup>-1</sup>.

### Forest soil

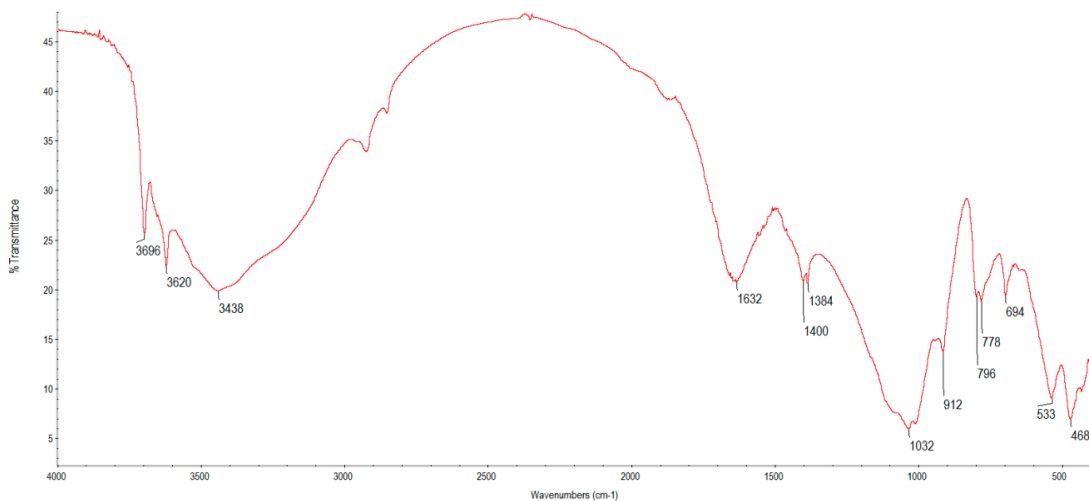


**Figure S1.** Infrared spectrum of forest soil.

The band at 3696 cm<sup>-1</sup> can be related to the presence of kaolinite, with bands at 3621 and 912 cm<sup>-1</sup> being typical for clay minerals [6]. Saikia and Parthasarathy [17] also indicate that a typical spectrum of kaolin should present bands at 3697 and 3620 cm<sup>-1</sup> (among other). Taking into account that indicated by Haberhauer and Gerzabek [8], the band at 3438 cm<sup>-1</sup> would be due to stretching vibration of bonded and non-bonded hydroxyl groups, the one at 1632 would be related to C=O vibrations of carboxylates and aromatic vibrations, although it could be related to H-O-H bending of water [17]. Tinti et al.[23] indicate that a band at approximately 1400 cm<sup>-1</sup> is present in different clay materials, whereas a band at about 1380 cm<sup>-1</sup> would be due to coordinatively bound water. As per Margenot et al. [10], a single broad peak at 1030–1010 cm<sup>-1</sup> can be related to the 2:1 layer silicates. Haberhauer and Gerzabek [8] also indicate that a band at about 1050 would be indicative of polysaccharides, or of Si-O vibrations of clay minerals, and bands at about 780, 690 and 540 cm<sup>-1</sup> would be due to clay, quartz minerals or other inorganic materials.

### Vineyard soil

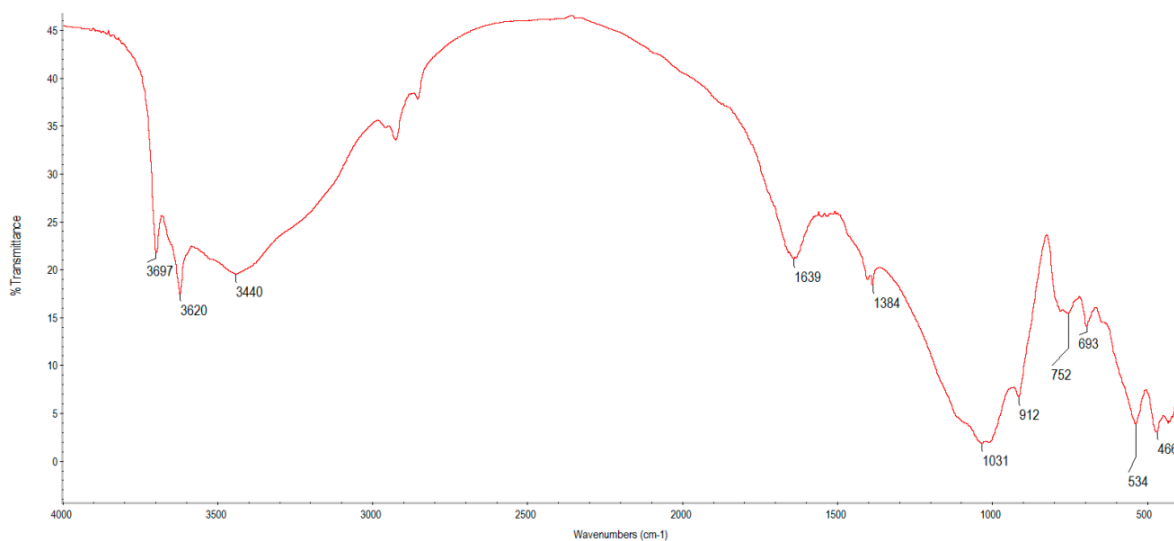


**Figure S2.** Infrared spectrum of vineyard soil.

As in the case of the forest soil, the band at  $3697\text{ cm}^{-1}$  would be related to the presence of kaolinite, with this band and those at  $3620$  and  $912\text{ cm}^{-1}$  being typical for clay minerals [6]. The band at  $3440\text{ cm}^{-1}$  would be due to H-O-H stretching of adsorbed water [17], whereas the band at  $1639\text{ cm}^{-1}$  could be related to H-O-H bending of water (although it could be related to C=O vibrations of carboxylates and aromatic vibrations; [8]). As per Sila et al. [18], a band at about  $1639\text{ cm}^{-1}$  would be due to the clay mineral montmorillonite. Tinti et al. [23] indicate that a band at about  $1380\text{ cm}^{-1}$  would be due to coordinatively bound water. Saikia and Parthasarathy [17] indicate that a band at about  $1031\text{ cm}^{-1}$  could be assigned to Si-O stretching of clay minerals. As per Margenot et al. [10], a single broad peak at  $1030$ – $1010\text{ cm}^{-1}$  can be related to the 2:1 layer silicates. The vineyard soil also showed bands at  $693$ ,  $534$ , and  $466\text{ cm}^{-1}$ , coincident or very close to bands present in the forest soil, and again some of them could be related to that indicated by Haberhauer and Gerzabek [8]: specifically, bands at about  $690$  and  $540\text{ cm}^{-1}$  would be due to clay, quartz minerals or other inorganic materials.

### Pyritic material

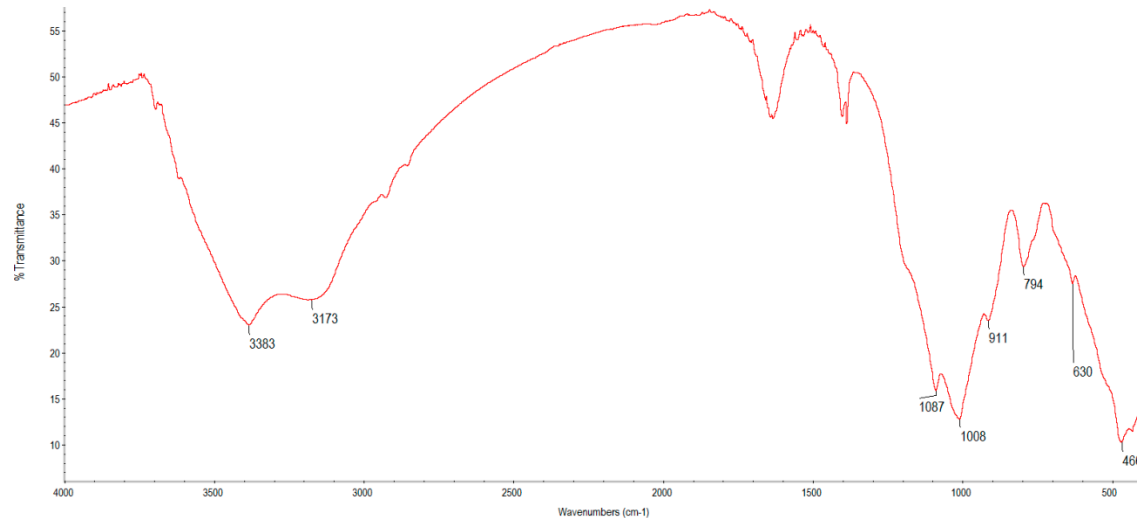


**Figure S3.** Infrared spectrum of pyritic material.

In the pyritic material, the band at  $3383\text{ cm}^{-1}$  may be related to O-H and N-H stretching, and H-bonded OH [10,23], the band at  $1087\text{ cm}^{-1}$  may be due to S-O bonds, or to phosphate [15]. Alejano et al. [1] indicated that characteristic SO functional group bands (corresponding to sulfate), placed at about  $474$ ,  $512$ ,  $871$  and  $977\text{ cm}^{-1}$ , can be detected both in non-altered and altered pyrite, whereas a band at about  $3600\text{ cm}^{-1}$  can be related to OH groups in coordination with metals, which would be due to iron hydroxides (frequent in altered pyrite).

### Fine mussel shell

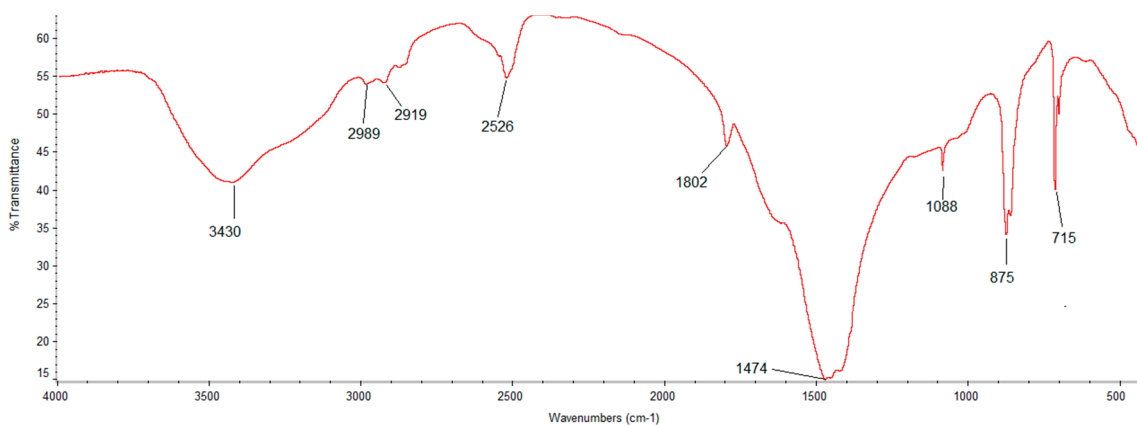


**Figure S4.** Infrared spectrum of fine mussel shell.

The band at  $3430\text{ cm}^{-1}$  may be related to N-H bonds, and at  $2989$  and  $2919\text{ cm}^{-1}$  to C-H groups. At  $2526\text{ cm}^{-1}$  it may be related to the presence of carbonate groups [13,19]; The band at  $1802\text{ cm}^{-1}$  may be related to the presence of C=O bindings in acids [15]. At  $1474\text{ cm}^{-1}$  may be due to CH<sub>2</sub>- bonds, and at  $1088\text{ cm}^{-1}$  to S-O bonds, or to phosphates [15]. The band at  $875\text{ cm}^{-1}$  could be due to C-O bonds in carbonates, and at  $715\text{ cm}^{-1}$  to N-H bonds [13, 19].

### Pine bark

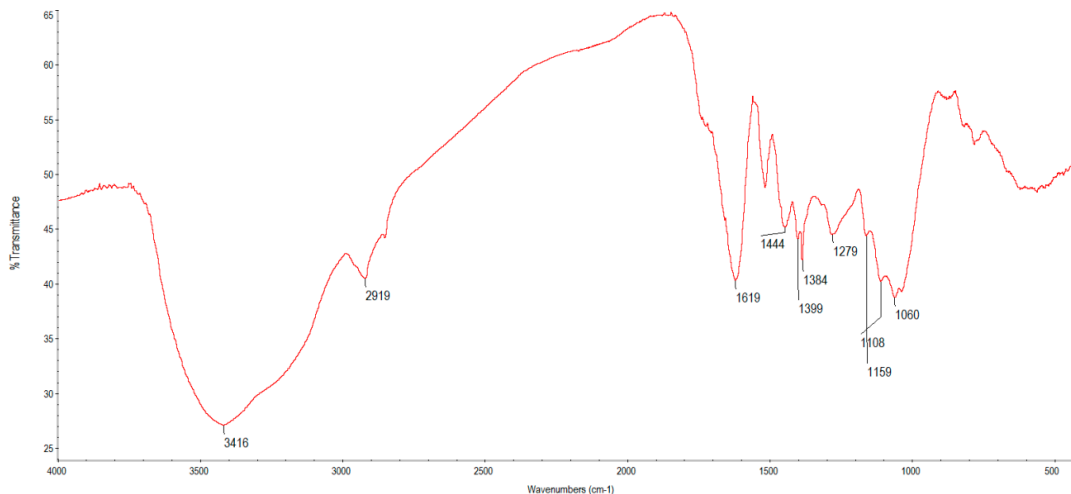


**Figure S5.** Infrared spectrum of pine bark.

In the case of pine bark, FTIR spectrum shows details very similar to those previously found by Brás et al. [3]. Specifically, the band at  $3416\text{ cm}^{-1}$  would be due to the bond between the oxygen and the hydrogen stretching vibration; the one at  $2919$  would correspond to the stretching C-H bond in the aromatic and aliphatic structures; the one situated at  $1619$  would be due to the aromatic C=C skeletal vibrations; the band at  $1444$  would be caused by C-H deformation; and the one at  $1159$  would be in relation to the asymmetric stretching of C-O-C in cellulose and hemicellulose [3] Fackler et al. [7] indicate that the band at  $1108$  may correspond to ring asymmetric valence vibration of polysaccharides, whereas the band at  $1060$  may be due to C<sub>3</sub>-O<sub>3</sub>H valence vibration, mainly from polysaccharides.

### Oak ash

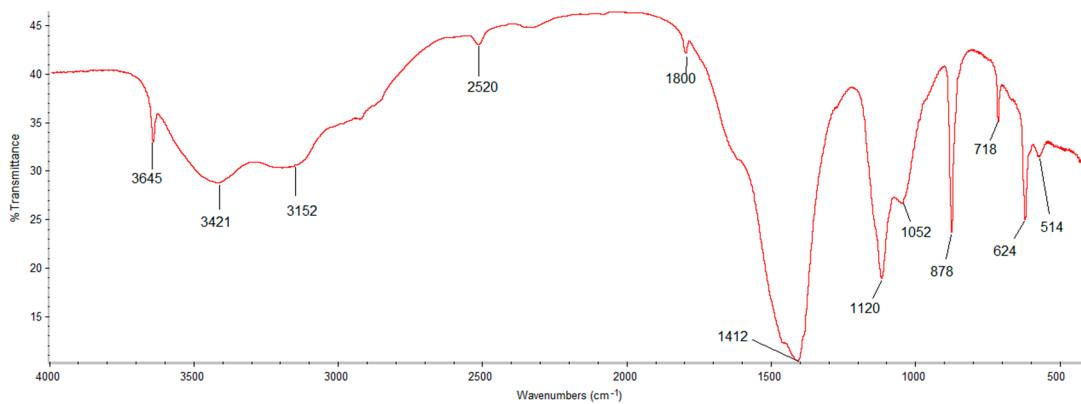


**Figure S6.** Infrared spectrum of oak ash.

The band at  $3645\text{ cm}^{-1}$  can be related to O-H stretching for some primary alcohol structures [15]. The band in the  $3421\text{ cm}^{-1}$  region can be attributed to O-H and N-H bonds, due to the presence of hydroxyl, carboxyl, amine and amide groups [13,15,19] The band at  $3152\text{ cm}^{-1}$  may be related to the

stretching of N-H groups of amines and primary and secondary amides [15].. Stretching at  $2520\text{ cm}^{-1}$  may be related to O-H bonds in carboxylic acids [15]. or to carbonates [19]. The band at  $1800\text{ cm}^{-1}$  may be related to the presence of C=O binding in acids [15].. At  $1412\text{ cm}^{-1}$ , to the presence of nitrates, and C-N, N-H and C-H bonds [13,19] or also to folding deformation of -CH<sub>3</sub> in alkane groups. The band at  $1120\text{ cm}^{-1}$  may be related to the presence of fluoride, C-N-bond amines, or C-O bonds of alcohols, or carboxylic acids [15]. It may also be related to C-O-C, C-O, or C-O-P bonds [13,19]. The band at  $1052\text{ cm}^{-1}$  can suggest a C-O bond, phosphate groups [13,19]and sulfoxides [15], whereas the band at  $878\text{ cm}^{-1}$  can be due to C-O bonds in carbonates. The band at  $718\text{ cm}^{-1}$  can be due to N-H bonds, at  $624\text{ cm}^{-1}$  may be due to S-O bonds, and at  $514\text{ cm}^{-1}$  may be C=C bonds [13,19].

### Hemp waste

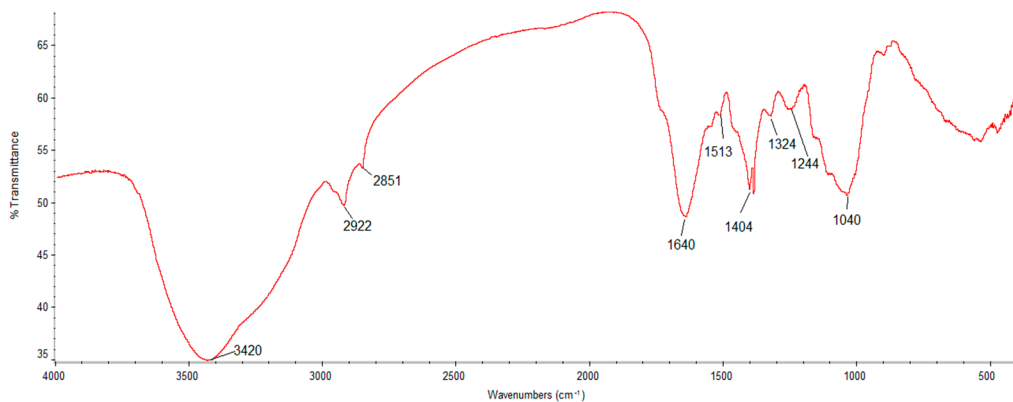


**Figure S7.** Infrared spectrum of hemp waste.

The wide band in the  $3420\text{ cm}^{-1}$  region can be attributed to stretching vibration of the O-H bond, suggesting the presence of hydroxyl groups (OH) found in cellulose, lignin and water [16,19,22]. The bands at  $2922$  and  $2851\text{ cm}^{-1}$  can be related to the stretching vibration of C-H and CH<sub>2</sub> of alkane and aliphatic acids groups [13], also found in cashew nut shell [5]. The band at  $1640\text{ cm}^{-1}$  can be attributed to C=C bonds in alkenes, or to C=O bonds in amides [15]. The band at  $1513\text{ cm}^{-1}$  can be related to a CH bond in a phenolic ring in lignin [13]. A folding -CH<sub>3</sub> deformation can be found at  $1404\text{ cm}^{-1}$ , relating to alkane groups [15]. According to these authors, C-N bonds corresponding to aromatic amines can be found in the region  $1324\text{ cm}^{-1}$ . The stretching in the frequencies  $1244$  and  $1040\text{ cm}^{-1}$  can be attributed to the presence of asymmetric phosphate groups, C-O of carboxylic acids, and C-O-C, C-O, C-O-P of polysaccharides [13,15,19].

### References

- Alejano, L.R., Pericho, A., Olalla, C., Jiménez, R. 2014. Rock Engineering and Rock Mechanics: Structures in and on Rock Masses. CRC Press. London, 372 pp.
- Álvarez, E., Fernández-Sanjurjo, M.J., Núñez, A., Seco, N., Corti, G. 2012. Aluminium fractionation and speciation in bulk and rhizosphere of a grass soil amended with mussel shells or lime. Geoderma 173/174, 322–329.
- Brás, I., Teixeira-Lemos, L., Alves, A., Pereira, M.F.R. 2004. Application of pine bark as a sorbent for organic pollutants in effluents. Management of Environmental Quality: An International Journal 15(5), 491–501.
- Chatterjee, A., Lal, R., Wielopolski, L., Martin, M.Z., Ebinger, M.H. 2009. Evaluation of Different Soil Carbon Determination Methods. Critical Reviews in Plant Science 28, 164–178.
- Coelho, G.F., ConÇalves Jr., A.C., Tarley C.R.T., Casarin, J., Nacke, N., Francziskowski, M.A. 2014. Removal of metal ions Cd (II), Pb (II) and Cr (III) from water by the cashew nut shell *Anarcadium occidentale* L. Ecol. Eng. 73, 514–525.
- Dlapa, P., Bodí, M.B., Mataix-Solera, J., Cerdà, A., Doerr, S.H. 2013. FT-IR spectroscopy reveals that ash water repellency is highly dependent on ash chemical composition. Catena 108, 35–43.

7. Fackler, K., Stevanic, J.S., Ters, T., Hinterstoisser, B., Schwanninger, M., Salmén, L. 2010. Localisation and characterisation of incipient brown-rot decay within spruce wood cell walls using FT-IR imaging microscopy. *Enzyme and Microbial Technology* 47(6), 257–267.
8. Haberhauer, G., Gerzabek, M.H. 1999. Drift and transmission FT-IR spectroscopy of forest soils: an approach to determine decomposition processes of forest litter. *Vibrational Spectroscopy* 19(2), 413–417.
9. Kamprath, E.J. 1970. Exchangeable aluminium as a criterion for liming leached mineral soils. *Soil Science Society of America Proceedings* 34, 252–54.
10. Margenot, A.J., Calderón, F.J., Goyne, K.W., Mukome, F.N.D., Parikh, S.J. 2017. IR Spectroscopy, Soil Analysis Applications. *Encyclopedia of Spectroscopy and Spectrometry*, Third Edition, vol. 2, pp. 448–454.
11. McLean, E.O. 1982. Soil pH and Lime Requirement. In *Methods of Soil Analysis*, Part 2, Chemical and Microbiological Properties, ASA: Madison, USA, pp. 199–223.
12. Mimura, A.M.S., Vieira, T.V.A., Martinelli, P.B., Gorgulho, H.F. 2010. Utilization of rice husk to remove Cu<sup>2+</sup>, Al<sup>3+</sup>, Ni<sup>2+</sup> and Zn<sup>2+</sup> from wastewater. *Química Nova* 33(6), 1279–1284.
13. Movasaghi, Z., Rehman, S., Rehman, I. 2008. Fourier Transform Infrared (FTIR) Spectroscopy of Biological Tissues. *Applied Spectroscopy Reviews*, 43(2), 134–179.
14. Nóbrega, J.A., Pirola, C., Fialho, L.L., Rota, G., de Campos, C.E., Pollo, F. 2012. Microwave-assisted digestion of organic samples: How simple can it become? *Talanta* 98, 272–276.
15. Pavia, D.L., Lampman, G.M., Kriz, G.S., Vyvyan, J.R. 2010. *Introdução à espectroscopia*. 4<sup>a</sup> edição, São Paulo, Cengage Learning, 700 pp.
16. Rubio, F., GonÇalves Jr., A.C., Meneghel, A.P., Tarley, C.R.T., Schwantes, D., Coelho, G.F. 2013. Removal of cadmium from water using by-product *Crambe abyssinica* Hochst seeds as biosorbent material. *Water Science and Technology* 68(1), 227–233.
17. Saikia B.J., Parthasarathy, G. 2010. Fourier Transform Infrared Spectroscopic Characterization of Kaolinite from Assam and Meghalaya, Northeastern India. *J. Mod. Phys.* 1, 206–210.
18. Sila, A.M., Shepherd, K.D., Pokhriyal, G.P. 2016. Evaluating the utility of mid-infrared spectral subspaces for predicting soil properties. *Chemometrics and Intelligent Laboratory Systems*. 153, 92–105.
19. Smidt, W., Meissl, K. 2007. The applicability of Fourier transform infrared (FT-IR) spectroscopy in waste management. *Waste Management* 27, 268–276.
20. Sumner, M.E., Miller, W.P. 1996. Cation exchange capacity and exchange coefficients. In *Methods of Soil Analysis*, Part 3, Chemical Methods, ASA: Madison, USA, pp. 437–474.
21. Tan, K.H. 1996. Soil sampling, preparation, and analysis. Marcel Dekker: New York, USA.
22. Tarley, C.R.T., Arruda, M.A.Z. 2004. Biosorption of heavy metals using rice milling by-products. Characterisation and application for removal of metals from aqueous effluents. *Chemosphere* 54, 987–995.
23. Tinti, A., Tugnoli, V., Bonora, S., Francioso, O. 2015. Recent applications of vibrational mid-Infrared (IR) spectroscopy for studying soil components: a review. *Journal of Central European Agriculture* 16(1), 1–22.